JVSTB Journal of Vacuum Science & Technology B

Properties of sputtered Cr–O and reactively sputtered Cr–N–O as passivation layers against copper oxidation

Jui-Chang Chuang and Mao-Chieh Chen

Citation: Journal of Vacuum Science & Technology B **16**, 3021 (1998); doi: 10.1116/1.590336
View online: http://dx.doi.org/10.1116/1.590336
View Table of Contents: http://scitation.aip.org/content/avs/journal/jvstb/16/6?ver=pdfcov
Published by the AVS: Science & Technology of Materials, Interfaces, and Processing

Properties of sputtered Cr–O and reactively sputtered Cr–N–O as passivation layers against copper oxidation

Jui-Chang Chuang and Mao-Chieh Chen[a)]
Department of Electronics Engineering and the Institute of Electronics, National Chiao-Tung University, Hsinchu 300, Taiwan, Republic of China

(Received 8 October 1997; accepted 18 September 1998)

Passivation layers of 200 Å sputtered Cr–O as well as reactive sputtered Cr–N–O were studied with respect to the passivation capability against thermal oxidation of Cu in flowing nitrogen and flowing oxygen ambients. In a flowing N_2 ambient, both Cr–O and Cr–N–O passivation layers were able to prohibit oxidation of Cu at temperatures up to 700 °C. In an O_2 ambient, the passivation capability of Cr–N–O layer was found to be 500 °C, which is 150 °C higher than that of Cr–O layer. The superiority of the passivation capability of the Cr–N–O layer is presumably due to decoration of the surface defects and grain boundaries with nitrogen, which provide fast paths for oxygen and copper diffusion. © *1998 American Vacuum Society.* [S0734-211X(98)11706-7]

I. INTRODUCTION

Copper (Cu) has been studied extensively as a potential substitute for aluminum (Al) and Al alloys in multilevel metallizations of semiconductor devices.[1,2] Cu has beneficial factors compared with Al and Al alloys, such as low bulk resistivity[1,3] (1.7 vs 2.7 and >4.0 $\mu\Omega$ cm), high melting point,[3,4] high electromigration resistance,[5] and low reactivity with commonly used diffusion barrier materials.[1–5] However, there are unfavorable factors compared with Al and Al alloys, for example, poor adhesion to dielectric layers,[1] difficulty in dry etching,[6] fast diffusion in silicon and SiO_2, deep level trap in silicon, and formation of Cu silicides at low temperatures. All of these drawbacks have detrimental effects on devices reliability.[7–12] In addition, copper oxidizes easily and forms nonconductive compounds at temperatures below 150 °C.[13–16] Passivation layers against Cu oxidation have been studied, for example, self-aligned passivation by (Al, Mg),[17,18] (Ti, Cr),[19] and Nb,[20] sidewall passivation[21,22] by Mo and TiN, formation of surface silicide,[23] and B-implanted oxidation resistant Cu layer.[24]

Chromium (Cr) and its nitride films have been widely used as a scratch and corrosion passivation layer in field applications.[25,26] Thermodynamic data[3,27] show that it is easier to form Cr_2O_3 than copper oxides. Moreover, it has been shown that Cr_2O_3, which is the oxidation product of CrN and Cr_2N, is thermally stable at temperatures above 700 °C.[28] However, no study has been reported concerning the passivation capability of Cr-based films against oxidation of Cu layers for integrated circuit applications.

In this work, sputtered Cr–O and reactively sputtered Cr–N–O films were deposited on Cu surfaces. The Cr–O/Cu/SiO_2 and Cr–N–O/Cu/SiO_2 structures were thermally annealed in N_2 and O_2 ambients to investigate the passivation capability against Cu oxidation.

[a)]Electronic mail: mcchen@cc.nctu.edu.tw

II. EXPERIMENTAL PROCEDURE

The starting materials used for sample preparation were *p*-type, boron doped, 3-in.-diam Si wafers with a nominal resistivity of 17–55 Ω cm. After an initial RCA cleaning,[29] the Si wafers were thermally oxidized at 1050 °C in steam to grow 5000 Å of SiO_2. A 2000-Å-thick Cu film was sputter deposited on the oxide layer. This was followed by deposition of a 200 Å Cr or Cr oxynitride film on the Cu layer in the same sputtering system without breaking the vacuum. The Cr film was sputter deposited using a pure Cr target (99.999% purity) in an Ar ambient, while the Cr oxynitride films were deposited by reactive sputtering using the same Cr target in a gas mixture of Ar and N_2 with various flow rates. All the gases used were electronic grade. The base pressure of the deposition chamber was 1.0×10^{-6} Torr, and all films were deposited at a pressure of 7.8 mTorr without intentional substrate heating. Since Cr is an inherent oxygen absorber[4,27] and the base pressure of the deposition chamber was only modestly low, oxygen was inevitably incorporated into the deposited layers, leading to either Cr–O or Cr–N–O films. Table I summarizes the sample identification, sputtering condition, and some specific parameters for the sputtered Cr and Cr oxynitride films. The atomic concentrations of nitrogen and oxygen were determined by Auger electron spectroscopy (AES) analysis. Wafers were diced into 1.5 $\times1.5$ cm^2 pieces for further treatment. The diced samples were thermally annealed in a flowing N_2 ambient for 30 min, or in a flowing O_2 ambient for 50 min at temperatures ranging from 100 to 700 °C for the passivation studies. Electrical measurements and material analysis were used to characterize the passivation capability. Sheet resistance (R_S) was measured using a four-point probe. Film thicknesses were measured using an α-step profiler and scanning electron microscope (SEM). A SEM was also used to investigate surface morphology. X-ray photoelectron spectroscopy (XPS) and x-ray diffraction (XRD) analysis were used for phase identification. Secondary ion mass spectroscopy (SIMS) was used for depth profile analysis.

TABLE I. Deposition conditions and specific parameters of as-deposited Cr–O and Cr–N–O films.

Sample identification	A (Cr–O)	B (Cr–N–O)	C (Cr–N–O)
Partial pressure of N_2 in sputtering gas (mTorr)	0	0.195	1.56
Deposition power (W)	100	150	150
Deposition rate (Å/s)	0.3	0.4	0.4
Resistivity ($\mu\Omega$ cm)	8.7	7.5	5.3
Nitrogen atomic concentration (%)	0[a]	0[a]	30
Oxygen atomic concentration (%)	35	35	25

[a]Below detection limit.

III. RESULTS AND DISCUSSION

A. As-deposited Cr–O and Cr–N–O films

Figure 1 shows the surface morphology of the as-deposited Cr–O and Cr–N–O films. Cracks can be seen on the surface of sample A [Fig. 1(a)] and sample B [Fig. 1(b)],

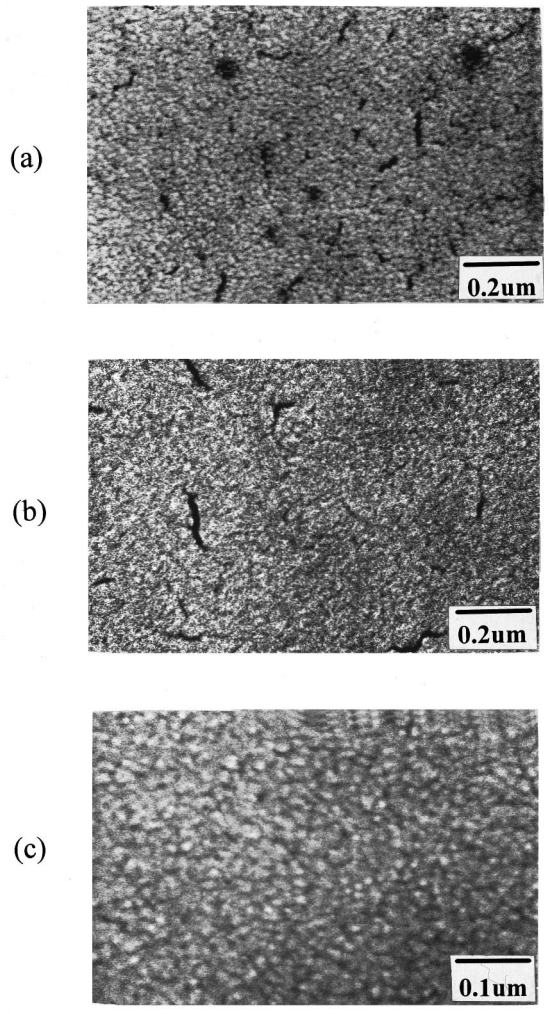

FIG. 1. SEM micrographs showing surface morphology of as-deposited (a) sample A, (b) sample B, and (c) sample C.

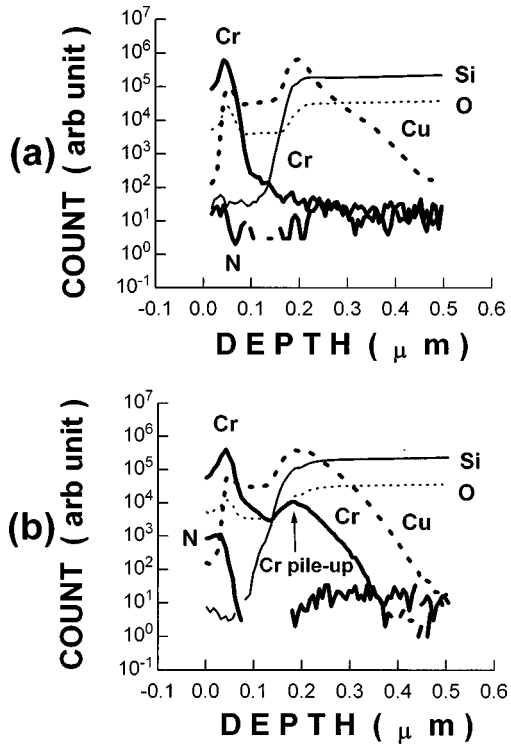

FIG. 2. SIMS depth profiles for sample A (a) as-deposited and (b) 500 °C N_2 annealed.

which were, respectively, not doped and lightly doped with nitrogen. For the nitrogen doped sample C, a smooth surface was observed [Fig. 1(c)]. The surface morphology of the Cr–O film can be improved by nitrogen incorporation.

XPS[30] analysis indicated that oxygen was present throughout the Cr–O and Cr–N–O films, but not in the underlying Cu layer. (The XPS instrument used in this study was the model: ESCA PHI 1600 of Perkin Elmer. All the XPS binding energies were calibrated using the binding energy of surface absorbed carbon C 1*s* photoelectrons, which is 284.5 eV.[30]) The nitrogen of both samples B and C was determined to be in the Cr nitride (Cr_2N) phase based on the binding energy of N 1*s* photoelectrons measured to be 397.4 eV. On the top surface, Cr $2p_{3/2}$ and O 1*s* photoelectrons were utilized to determine that oxygen was present only in the Cr_2O_3 phase, whose binding energies were determined to be 576.8 and 531.4 eV, respectively, presumably resulting from the air exposure. However, inside the Cr–O and Cr–N–O layers for all samples, only unreacted oxygen was present based on Cr $2p_{3/2}$ and O 1*s* photoelectron binding energies of 574.4 and 531.0 eV, respectively.

The oxygen and nitrogen contents, as determined by AES analysis, along with the resistivity, as determined from the sheet resistance and thickness measurements, are tabulated in Table I for the as-deposited films. It can be seen that nitrogen incorporation resulted in reduced resistivity.

B. Thermal annealing in N_2 ambient

Figures 2 and 3 show the SIMS depth profiles for the as-deposited as well as the 500 °C annealed samples A and

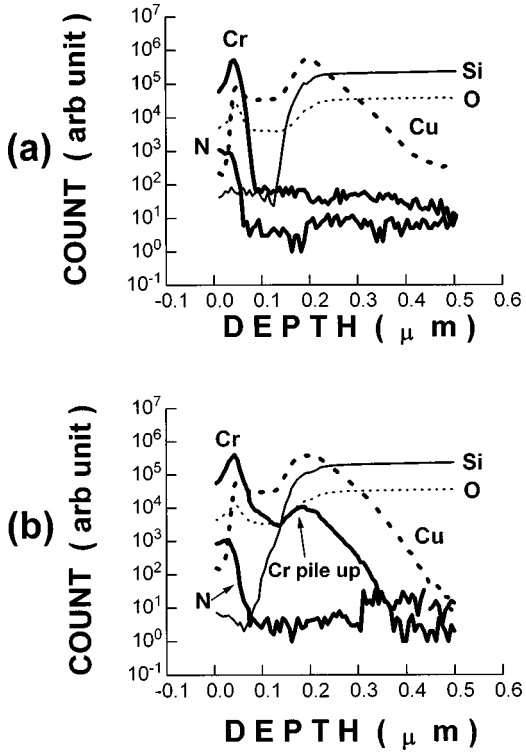

FIG. 3. SIMS depth profiles for sample C (a) as-deposited and (b) 500 °C N_2 annealed.

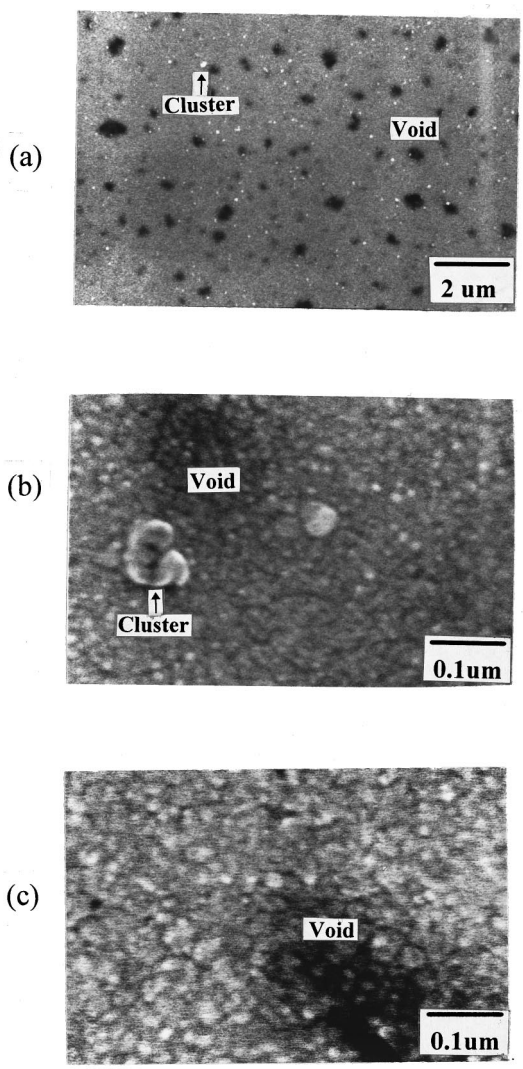

FIG. 4. SEM micrographs showing surface morphology for sample B annealed at (a) and (b) 500 °C, and (c) 700 °C. The micrographs (b) and (c) have a 20 times magnification of micrograph (a).

C, respectively. (The penetration of Cu into SiO_2 is commonly observed because there is no barrier layer separating the sputter deposition of Cu on the SiO_2 substrate.) For sample A, the Cu profile remained nearly unchanged after annealing [Fig. 2(b)] as compared with the as-deposited profile [Fig. 2(a)], while the N and Cr profiles revealed significant change. The N signal in the passivation layer of the annealed sample increased two orders of magnitude over the as-deposited film. The Cr profile reveals a Cr pileup at the Cu/SiO_2 interface. For sample C (Fig. 3), N_2 annealing did not change the Cu or N profile, while a similar pileup of Cr was found at the Cu/SiO_2 interface.

The 500 and 700 °C annealed samples of B as well as C were analyzed by XPS.[30] Similar results were obtained for the B and C samples. Based on the measured binding energies of Cr $2p_{3/2}$, N 1*s*, and O 1*s* photoelectrons, we determined that the Cr in the Cr–N–O layer was a mixture of elemental and nitride (Cr_2N) states, and only unreacted oxygen was present throughout the entire passivation layer. Because no copper signal was found in the passivation layers, thermal annealing in N_2 only nitrided the passivation layer of sample B, and presumably only sintered that of sample C; these nitrided and/or sintered passivation layers protected the underlying Cu layer from being oxidized by the oxygen incorporated in the passivation layer and the residual oxygen in the annealing ambient.

Figure 4 shows the surface morphology of sample B following annealing in a N_2 ambient. Figures 4(a) and 4(b) are following a 500 °C anneal with Fig. 4(b) a 20× magnification of Fig. 4(a). Figure 4(c) shows the surface morphology following a 700 °C N_2 anneal. Similar cluster and void formation was observed on the annealed samples of A and B. For sample B annealed at 700 °C, clusters were no longer visible, as shown in Fig. 4(c). Figure 5 shows the surface morphology of sample C annealed in a N_2 ambient at various temperatures; voids are clearly observed on the surface, but clusters did not appear.

Voids were observed for all samples thermally annealed in a N_2 ambient at elevated temperatures. Voids (Figs. 4 and 5) could arise from the agglomeration of the film due to the mismatch of the thermal expansion coefficient between Cr–N–O and Cu as well as the volume difference of Cr and Cr_2N. Another possibility is the Kirkendall effect[31] resulting from the higher diffusivity of Cr as compared with Cu.[3,27] This could result in the movement of more Cr than Cu, leading to a coalescence of vacancies into voids. The movement of Cr could explain the Cr pileup at the Cu/SiO_2 interface observed in the SIMS profiles.

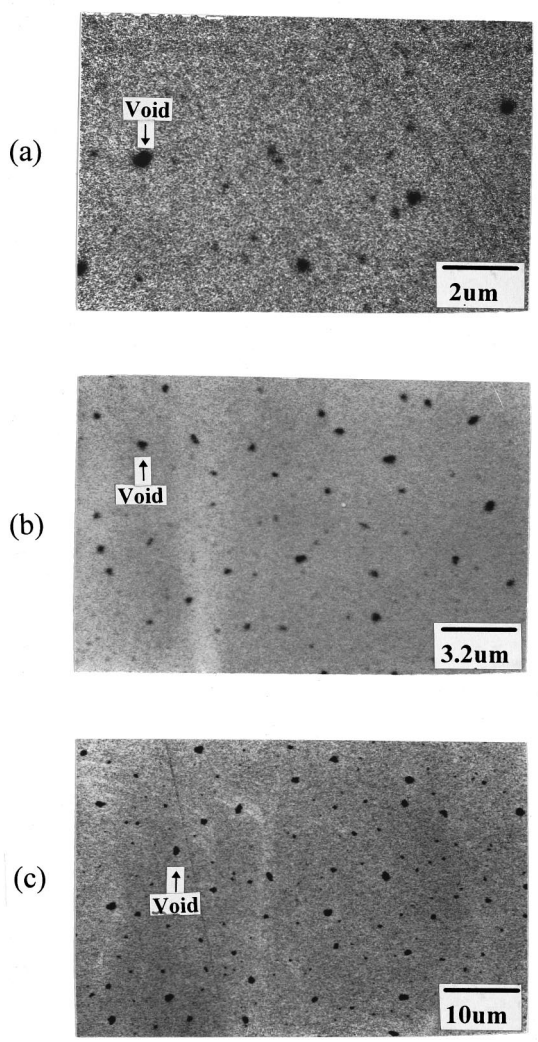

FIG. 5. SEM micrographs showing surface morphology for sample C annealed at (a) 400 °C, (b) 500 °C, and (c) 700 °C in N_2 ambient.

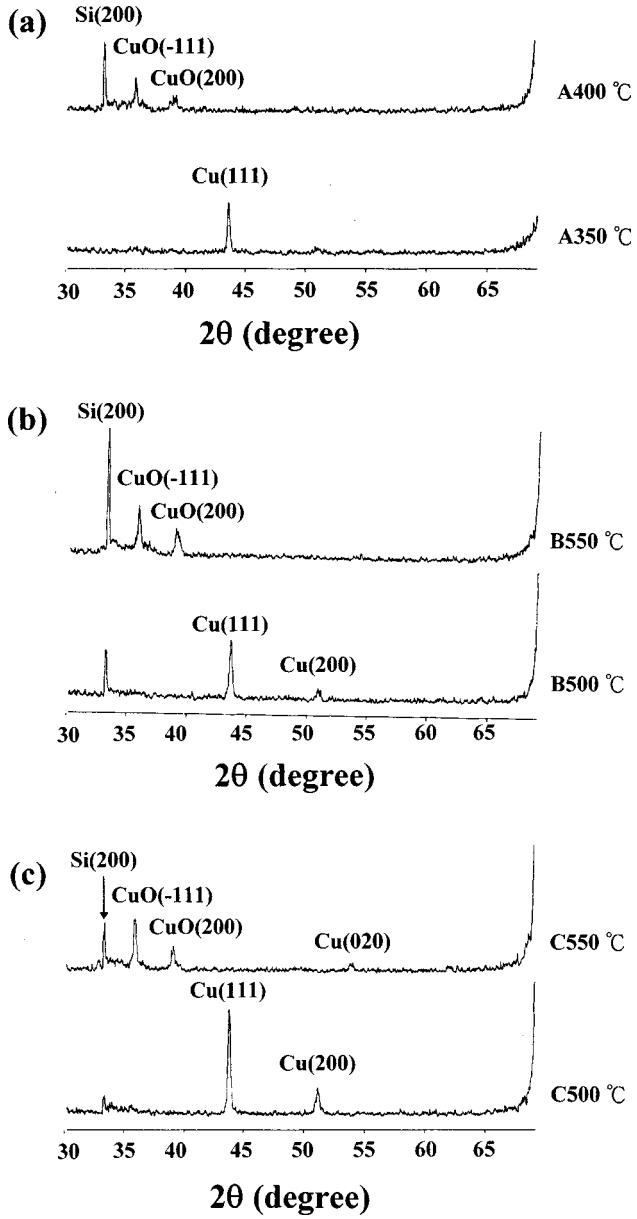

FIG. 6. XRD spectra for (a) sample A, (b) sample B, and (c) sample C thermally annealed in O_2 ambient at temperatures below as well as above their respective temperatures of Cu oxide appearance.

For samples A and B, which were nitrogen deficient in the as-deposited passivation layers, the nitrogen for doping and/or nitridation came from the flowing N_2 ambient during the thermal N_2 annealing. It was easier to form Cr nitride on the film surface than inside the film because there were many more nucleation sites on the surface. Thus, the clusters that were observed in low temperature annealed samples A and B [Figs. 4(a) and 4(b)] were presumed to be Cr_2N. As the annealing temperature was raised high enough, the Cr_2N clusters nucleated into a continuous layer, thus no cluster was observed [Fig. 4(c)]. For sample Cs, whose Cr–N–O passivation layers contained plenty of nitrogen, thermal N_2 annealing resulted in little change in the N profile (Fig. 3) and no clusters were observed (Fig. 5); this is because the nucleation of Cr nitride occurred mostly inside the nitrogen sufficient Cr–N–O layer.

The electrical resistivity of all samples annealed in a N_2 ambient reached a low value of approximately 3 $\mu\Omega$ cm, which was determined simply by taking the product of measured sheet resistance and the layer thickness measured from the outermost surface to the Cu/SiO_2 interface. The resistivity is very likely overestimated using this approach. Since 1% (atomic concentration) an increase of Cr in Cu would result in about a 4 $\mu\Omega$ cm resistivity increase,[3,4,32] we estimate that less than 1% of the Cr diffused into the Cu after N_2 annealing at 700 °C.

No Cu oxide was detected for any of the samples (A, B, and C) annealed in a N_2 ambient at temperatures up to 700 °C by the analytical instruments used in this study. Instead, the thermal N_2 annealing results in nitridation and sintering.

C. Thermal annealing in O_2 ambient

Figure 6 shows the XRD spectra for the samples thermally annealed in an O_2 ambient at temperatures below as

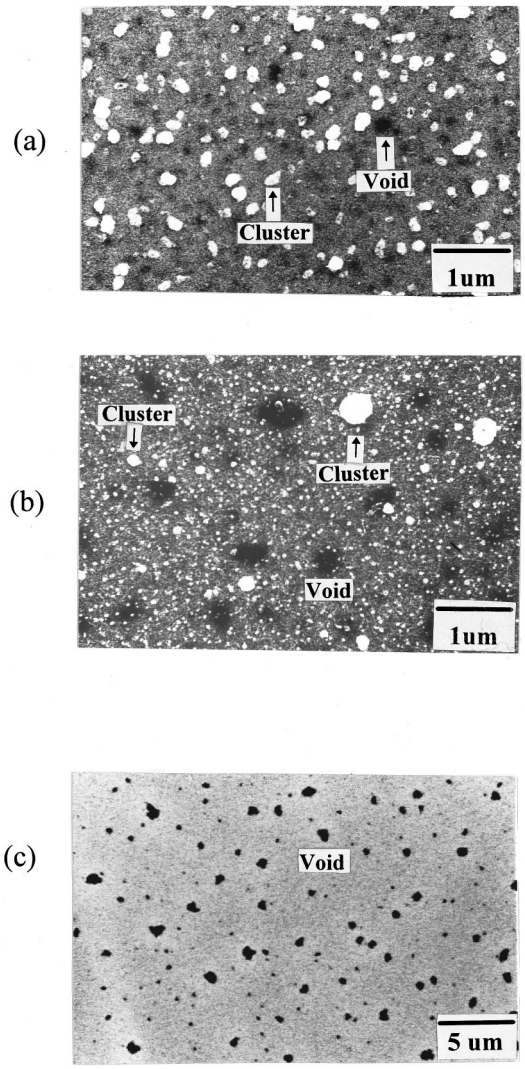

FIG. 7. SEM micrographs showing surface morphology for the samples annealed in O_2 ambient (a) sample A annealed at 250 °C, (b) sample B annealed at 450 °C, and (c) sample C annealed at 500 °C.

well as above the temperature of copper oxide phase appearance. For sample A, which is a Cr–O layer without nitrogen doping, the effective range of passivation against Cu oxidation was found to be below 400 °C [Fig. 6(a)]. For sample B, which is a Cr–N–O layer with very low level nitrogen doping, the effective range of passivation against Cu oxidation was raised to 500 °C [Fig. 6(b)]. For sample C, which is a Cr–N–O layer with a high level of nitrogen doping, the effective range of passivation against Cu oxidation was also found to be up to 500 °C [Fig. 6(c)].

Figure 7 shows the surface morphology for the samples annealed in an O_2 ambient. Low temperature (250 °C) annealing of sample A resulted in clusters and voids [Fig. 7(a)]. For sample B, clusters were not observed after annealing at temperatures below 450 °C, but appeared when the annealing temperature was raised to 450 °C [Fig. 7(b)]. For sample C, no clusters were found after annealing at temperatures up to 500 °C [Fig. 7(c)].

XPS analysis with sequential ion milling provided an in-

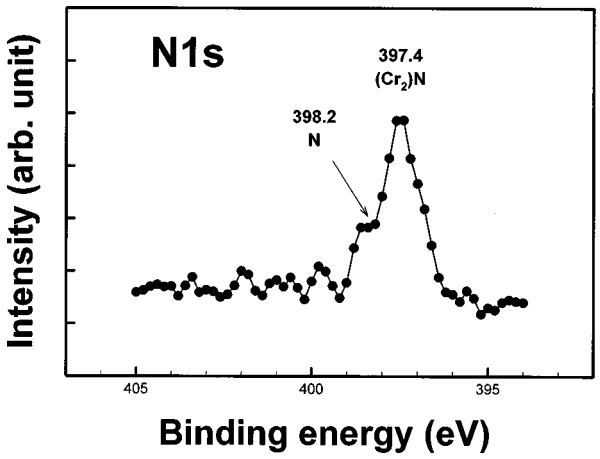

FIG. 8. Chemical states and binding energies of the N 1*s* photoelectrons for sample C annealed in O_2 ambient at 500 °C.

depth profile[30] of the 500 °C annealed sample B. On the outermost surface, the Cu $2p_{3/2}$, Cr $2p_{3/2}$, and O 1*s* photoelectrons, with binding energies at 934.0, 578.0, and 531.6 eV, respectively, were detected. As the surface region was sputter removed, the Cu $2p_{3/2}$ photoelectrons disappeared, while the binding energies of Cr $2p_{3/2}$ and O 1*s* photoelectrons shifted to 576.8 and 531.4 eV, respectively, which belong to the Cr_2O_3 state. The results indicated that a thin oxide ($CuCr_2O_4$) layer was present on the outermost surface followed by a much thicker underlying layer of Cr_2O_3. No N 1*s* photoelectron signal was detected. Moreover, the Cu $2p_{3/2}$ photoelectrons underneath the Cr_2O_3 layer remained in the elemental state, indicating no oxidation of the underlying Cu layer.

The results of XPS analysis with sequential ion milling for the 500 °C annealed sample C showed that the nitrogen was present in both the elemental and Cr_2N phases based on the N 1*s* photoelectron binding energies of 398.2 and 397.4 eV, respectively, as shown in Fig. 8. The surface was covered with a Cr_2O_3 outerlayer. A Cu signal was detected only underneath the Cr_2O_3 layer, and the Cu $2p_{3/2}$ photoelectrons underneath the Cr_2O_3 layer remained in the elemental state, indicating no oxidation of the Cu layer.

The surface defects provided easy diffusion paths[1,5,7–12] for oxygen and copper through the Cr–O layer, such as was the case for sample A shown in Fig. 1(a). With nitrogen incorporation into the passivation layer, the diffusion paths along the grain boundaries and the defects in samples B and C were decorated due to the nitrogen stuffing.[12,33] Moreover, thermal annealing in an O_2 ambient resulted in formation of Cr oxide[3,4,27,28] as well as healing of the defects and thus obstructing the diffusion of copper and oxygen. For sample B, however, because of the deficiency of nitrogen, Cu diffused to the surface through defects and reacted with Cr and oxygen to form $CuCr_2O_4$ on the outermost surface at the beginning of thermal annealing. As the diffusion paths of Cu were blocked by the formation of $CuCr_2O_4$ or impeded by the defect healing, oxidation of Cu ceased but oxidation of Cr continued.[3,4,27,28] For sample C, which has a much higher

level of nitrogen doping than sample B and has a very smooth surface morphology [Fig. 1(c)], annealing at 500 °C in O_2 ambient resulted in only Cr_2O_3 formation on the surface because there was no easy path for outdiffusion of Cu. Therefore, no copper oxide phase should be detected before the passivation layer was completely consumed, and the results of XPS analysis seem to support this presumption.

IV. SUMMARY AND CONCLUSION

Copper films passivated by a 200 Å sputter deposited Cr–O or reactively sputter deposited Cr–N–O layer were studied with respect to their passivation capability against thermal oxidation of Cu in flowing nitrogen and flowing oxygen ambients. The thermal N_2 annealing is essentially a nitridation and sintering process. The electrical resistivity of samples thermally annealed in N_2 reached a low value of about 3 $\mu\Omega$ cm, and we estimated that less than 1% (atomic concentration) of Cr resided in Cu after N_2 annealing at 700 °C. Both Cr–O and Cr–N–O passivation layers were able to prohibit oxidation of Cu at temperatures up to 700 °C. In an O_2 ambient, the passivation capability of Cr–N–O layer was found to be 500 °C, which is 150 °C higher than that of the Cr–O layer. Without nitrogen doping, there were cracks on the sputter deposited Cr–O layer, which presumably provided fast diffusion paths for oxygen and copper. With proper nitrogen doping, the reactive sputtered Cr–N–O layer has a very smooth surface morphology. We assume that the nitrogen doping resulted in the formation of Cr nitride in the Cr–N–O layers as well as decorated the diffusion paths, thus efficiently improving the passivation capability. Thermal annealing of the Cr–N–O/Cu/SiO_2/Si structure in an O_2 ambient indicated that the nitrogen doped Cr–N–O layer is effective in serving as a passivation layer against Cu oxidation up to 500 °C.

ACKNOWLEDGMENTS

The authors wish to thank the Semiconductor Research Center of National Chiao-Tung University for providing excellent processing environment. This work was supported by the National Science Council, Republic of China under Contract No. NSC-86-2215-E-009-040.

[1]See, for example, Mater. Res. Soc. Bull. 18 (1993); 19 (1994), devoted to the topic of Copper Metallization for Microelectronics.
[2]K. P. Rodbell, E. G. Colgan, and C.-K. Hu, Mater. Res. Soc. Symp. Proc. **337**, 59 (1994).
[3]*CRC Handbook of Chemistry and Physics*, 73rd ed., edited by D. R. Lide (CRC, Boca Raton, FL, 1992), Sec. 12.
[4]*Binary Alloy Phase Diagrams*, 2nd ed., edited by T. B. Massalski (ASM International, Material Park, OH, 1990), pp. 1266, 1293, 1304, and 1446.
[5]S. Shingubara, K. Fujiki, A. Sano, H. Sakaue, and Y. Horiike, Mater. Res. Soc. Symp. Proc. **338**, 441 (1994).
[6]Y. Igarashi, T. Yamanobe, and T. Ito, Thin Solid Films **262**, 124 (1995).
[7]J. D. McBrayer, R. M. Swanson, and T. W. Sigmon, J. Electrochem. Soc. **133**, 1242 (1986).
[8]Y. Shacham-Diamand, A. Dedhia, D. Hoffstetter, and W. G. Oldham, J. Electrochem. Soc. **140**, 2427 (1993).
[9]D. Gupta, Mater. Res. Soc. Symp. Proc. **337**, 209 (1994).
[10]G. Raghavan, C. Chiang, P. B. Anders, S. M. Tzeng, R. Villasol, G. Bai, M. Bohr, and D. B. Fraser, Thin Solid Films **262**, 168 (1995).
[11]*VLSI Technology*, 2nd ed., edited by S. M. Sze (McGraw-Hill, Singapore, 1988), p. 309.
[12]S. Q. Wang, S. Suthar, C. Hoeflich, and B. J. Burrow, J. Appl. Phys. **73**, 2301 (1993).
[13]J. Li, J. W. Mayer, and E. G. Colgan, J. Appl. Phys. **70**, 2820 (1991).
[14]M. O'Reilly, X. Jiang, J. T. Beechinor, S. Lynch, C. N. Dheasuna, J. C. Patterson, and G. M. Crean, Appl. Surf. Sci. **91**, 152 (1995).
[15]H. K. Liou, J. S. Huang, and K. N. Tu, J. Appl. Phys. **77**, 5443 (1995).
[16]A. J. Griffin, Jr., S. E. Hernández, and F. K. Brotzen, J. Electrochem. Soc. **141**, 807 (1994).
[17]W. A. Lanford, P. J. Ding, W. Wang, S. Hymes, and S. P. Murarka, Thin Solid Films **262**, 234 (1995).
[18]P. J. Ding, W. Wang, W. A. Lanford, S. Hymes, and S. P. Murarka, Appl. Phys. Lett. **65**, 1778 (1994).
[19]J. Li, J. W. Mayer, Y. Shacham-Diamand, and E. G. Colgan, Appl. Phys. Lett. **60**, 2983 (1992).
[20]H. Itow, Y. Nakasaki, G. Minamihaba, K. Suguro, and H. Okano, Appl. Phys. Lett. **63**, 934 (1993).
[21]D. S. Gardner, J. Onuki, K. Kudoo, Y. Misawa, and Q. T. Vu, Thin Solid Films **262**, 104 (1995).
[22]Y. Igarashi, T. Yamanobe, T. Yamaji, S. Nishikawa, and T. Ito, Jpn. J. Appl. Phys., Part 1 **33**, 462 (1994).
[23]S. Hymes, S. P. Murarka, C. Shepard, and W. A. Lanford, J. Appl. Phys. **71**, 4623 (1992).
[24]P. J. Ding, W. A. Lanford, S. Hymes, and S. P. Murarka, J. Appl. Phys. **74**, 1331 (1993).
[25]F. Cosset, G. Contoux, A. Celerier, and J. Machet, Surf. Coat. Technol. **79**, 25 (1996).
[26]C. Friedrich, G. Berg, E. Broszeit, and K.-H. Kloos, Surf. Coat. Technol. **74–75**, 279 (1995).
[27]E. A. Brandes, *Smithells Metals Handbook*, 6th ed. (Robert Hartnoll, Bodmin, Cornwall, England, 1983), pp. 8-21–8-25.
[28]T. Kacsich and K.-P. Lieb, Thin Solid Films **235**, 4 (1994).
[29]W. Kern and D. A. Puotinen, RCA Rev. **31**, 187 (1970).
[30]*Handbook of X-ray Photoelectron Spectroscopy*, edited by G. E. Muilenberg (Perkin-Elmer Physical Electronics Division, Eden Prairie, MN, 1979).
[31]R. E. Reed-Hill, *Physical Metallurgy Principles*, 2nd ed. (Van Nostrand, New York, 1972), pp. 386–390.
[32]C. Cabral, Jr., J. M. E. Harper, K. Holloway, D. A. Smith, and R. G. Schad, J. Vac. Sci. Technol. A **10**, 1706 (1992).
[33]J.-C. Chiou, K.-C. Juang, and M.-C. Chen, J. Electrochem. Soc. **142**, 2326 (1995).